An Improved Calculation Model for Analysis of [111] InGaAs/GaAs Strained Piezoelectric Superlattices

Byoung-Whi Kim[a)], Jea-Hoon Yoo, and Soo Hyung Kim

We present a calculation model for an improved quantitative theoretical analysis of electronic and optical properties of strained-piezoelectric [111] InGaAs/GaAs superlattices (SLs). The model includes a full band-coupling between the four important energy bands: conduction, heavy, light, and spin split-off valence bands. The interactions between these and higher lying bands are treated by the k · p perturbation method. The model takes into account the differences in the band and strain parameters of constituent materials of the heterostructures by transforming it into an SL potential in the larger band-gap material region. It self-consistently solves an 8 × 8 effective-mass Schrödinger equation and the Hartree and exchange-correlation potential equations through the variational procedure proposed recently by the present first author and applied to calculate optical matrix elements and spontaneous emission rates. The model can be used to further elucidate the recent theoretical results and experimental observations of interesting properties of this type of quantum well and SL structures, including screening of piezoelectric field and its resultant optical nonlinearities for use in optoelectronic devices.

Manuscript received August 12; revised Octorber 7, 1999.

[a)] Electronic mail: kbw@etri.re.kr

I. INTRODUCTION

Since Smith [1] predicted the existence of large piezoelectric fields in strained [111]-growth-axis semiconductor heterostructures in 1986, there has been intensive research on the physics [2]–[19] and opto-electronic device application of semiconductor heterostructures oriented in high index directions, especially in the [111] crystallographic direction [20]–[33]. In contrast to the strained quantum well (QW) structures grown along the [100] axis, strained layers grown other than [100] direction are piezoelectrically active and large built-in electronic fields can be generated [4].

Such strain-induced built-in electric fields provide extra degree of freedom for band-gap engineering and open possibilities of fabricating new or enhanced electrical and optical devices over the conventional [100]-oriented counterparts [4], [8]. Attractive features in this type of heterostructures include enhanced optical transitions, a reduced threshold current density of laser diode [34], [36], and large nonlinearity arising from the screening of the internal electric field by the photo-generated carriers.

The critical thickness along [111] were predicted [5], [14] to increase significantly as compared with that along [100] and the piezoelectric field is predicted to be strongest in this direction. Thus, the opportunity of tuning the electronic band structure as a function of the strain conditions is greater in [111] than in other directions. This flexibility is currently being exploited through the improvement or novel design of semiconductor diode lasers, electro-optical modulators, nonlinear optical devices, infrared imaging systems, etc [20]–[33].

The Stark shift induced by the piezoelectric field is the key reason that such structures have attracted much interest for use

in nonlinear optical devices. It has been shown that the Stark shift can be employed in the design of self electro-optic devices (SEEDs) using blue shift with reverse bias rather than red shift as in the case of conventional SEED [21]. This may lead to an enhancement in the operating characteristics of such devices. Also it has been suggested that the screening of the piezoelectric field could be utilized in new device structures; e.g., coupled waveguide structures could utilize a carrier density dependent refractive index to switch the wave between individual guides; and piezoelectric QW lasers operated under forward bias could be used in an integrated laser and blue-shifting waveguide electro-absorption modulator or an integrated laser and frequency-doubling waveguide. Thus, together with the quantum-confined Stark shift the strained-piezoelectric structure opens possibilities of making fully optically operated devices where the strain-induced built-in piezoelectric field within the QWs can be modulated by the incident optical signals.

Although it is well documented from the previous investigations that the screening of the piezoelectric fields by the photo-excited carriers should be responsible for the observed energy blue shift in these structures, there have been reported discrepancies between the theoretical and experimental results related to this phenomenon. Furthermore, it has been reported that in some structures the blue shifts may also arise from effects other than screening within the wells [10].

The most noticeable uncertainty is in the peizoelectric constant e_{14}: it has been suggested that the value of the piezoelectric constant obtained by linear interpolation should be reduced by 20 ~ 40 % depending on the In mole fraction. This is the simplest way to achieve reasonable agreements with the experimentally observed fields. However, the modifications are only qualitatively similar and the origin of the discrepancies between various groups is still unclear. This discrepancy may be due to errors in the nominal values used in the calculations (e.g., values of e_{14} for GaAs are quoted, which vary from 0.12 to 0.21 C/m) or to the effects of strain on the materials constants. [10], [37]

On the other hand, most of the previous theoretical work has been done based on rather simplified theoretical models rather than taking into account a full interband coupling between the bands involved in the interband optical transitions and difference in band/strain parameters of constituent materials. In those simplified models, where many parameters such as the piezoelectric field, the strain, and the effective masses were adjusted to fit the experimental data, all physical trends can be reproduced, but a quantitative agreement may not be found without taking into account all the factors mentioned above. It may be also possible that these simplifications partly cause the discrepancies.

Furthermore, the magnitude of the blue shift needed for the application to optical devices is in the range of a few nm or a few meV. Design of such devices requires more refined knowledge of the behavior of QW structures with various structural and material parameters, particularly including the effects of high densities of charge carriers which result in non-square wells and the screening of the internal piezoelectric field by those injected carriers. Thus it becomes necessary to have a more refined calculation model for performing more quantitative analysis of these properties.

To this end, we present a comprehensive, detailed solution procedure for obtaining more exact electronic and optical properties of strained-piezoelectric QW and superlattice (SL) systems based on the envelope function equation and the variational method we recently proposed [38].

The SL wave function and corresponding effective-mass equation are formulated in terms of a linear combination of Bloch states of the material with the smaller band gap. In this formulation, the difference in bulk Bloch states and band parameters between constituent materials are transformed to be an SL potential in the larger band-gap material region, so that the effective-mass equation can be solved as a whole. Thus, the symmetry of SL and the current-continuity at the interfaces are implicitly taken into account through the order in perturbation theory [39] at which the bulk Bloch function at **k** is obtained in terms of the zone-center Bloch functions.

In the present work the Poisson's equation is reviewed for calculation of the Hartree potential for general, not symmetric QW systems, and relevant boundary conditions are derived. For taking into account the renormalization of the band gap due to high carrier densities, we present a slightly different calculation model of exchange-correlation potential for the two-component electron and hole system within the local density approximation. The model self-consistently solves an 8×8 Schrödinger equation [40] and the Hartree and exchange-correlation [41], [42] potential equations to obtain the subband energy structure and envelope functions, which in turn are used to calculate optical matrix elements and spontaneous emission rates.

As an illustration of application of the present model, and also to briefly investigate the effect of piezoelectric field on electronic and optical properties of the QW structure, we perform computations on a strain-induced piezoelectric GaAs/InGaAs SL with well/barrier thicknesses of 100 Å/100 Å and In mole fraction of 12 %. Comparison is made between the present result and experimental result [25] reported previously.

The paper is organized in the following way. Sections II–V present solution procedures for electronic properties. Sections VI and VII provide those for optical properties. The results of sample calculations are presented in Section VIII. Conclusions are followed finally.

II. ENVELOPE FUNCTION EQUATION

The one-particle SL effective-mass equation for envelope function ψ can be expressed as [38]

$$\mathsf{E}\,\psi(\nu,\mathbf{k}_t,n,q;z)=\sum_{\nu'}\left[H_{\nu\nu'}(\mathbf{k}_t,-i\partial_z)+W_{\nu\nu'}(\mathbf{k}_t,-i\partial_z)\right]\psi(\nu',\mathbf{k}_t,n,q;z), \tag{1}$$

where n is SL subband index, q the wave vector associated with the SL growth direction (z-direction), and $\mathbf{k}_t$ the in-plane wave vector. The "fundamental" term $H_{\nu\nu'}$ and the "SL potential term" $W_{\nu\nu'}$ are defined, respectively, as

$$H_{\nu\nu'}(\mathbf{k},\mathbf{k}')\cong\left(\mathsf{E}^{A}_{\nu,0}+\frac{\hbar^2k^2}{2m_0}\right)\delta_{\nu\nu'}\delta_{\mathrm{k},\mathrm{k}'}+L^{A}_{\nu\nu'}\delta_{\mathrm{k},\mathrm{k}'}, \tag{2}$$

$$W_{\nu\nu'}(\mathbf{k},\mathbf{k}')\cong\int dz e^{i(k'_z-k_z)z}\theta^{B}_{z}\left[\left(\mathsf{E}^{B}_{\nu,0}-\mathsf{E}^{A}_{\nu,0}\right)+\left(L^{B}_{\nu\nu'}-L^{A}_{\nu\nu'}\right)\right]\delta_{\mathrm{k}_t,\mathrm{k}'_t}, \tag{3}$$

where A(B) represent a constituent material with smaller (larger) bandgap, and

$$L_{\nu\nu'}(\mathrm{k})\equiv\frac{\hbar}{m_0}\langle\nu,0|\,\mathbf{k}\cdot\mathbf{p}\,|\nu',0\rangle+\left(\frac{\hbar}{m_0}\right)^2\sum_{N\neq J}\frac{\langle\nu,0|\,\mathbf{k}\cdot\mathbf{p}\,|N,0\rangle\langle N,0|\,\mathbf{k}\cdot\mathbf{p}\,|\nu',0\rangle}{\mathsf{E}_{\nu,0}-\mathsf{E}_{N,0}}, \tag{4}$$

with J consisting of the primary bands with band index ν.

Note that in Eqs. (1)–(3) we employ a basis set of material A to describe the states for both constituent materials, and we assume that the coefficient of c^{η}_{ν} which represents overlap of the Bloch functions between the materials A and B $c^{\nu'}_{\nu}={}^{B}\langle\nu',0|\nu,0\rangle^{A}$, where ν' and ν are band indices of the bulk, can be approximated as $c^{\eta}_{\nu}=\delta_{\nu,\eta}$, while keeping the difference in band and strain parameters in the equation.

Upon including the four most important bands (the conduction, heavy-hole, light-hole, and spin split-off bands), $H_{\nu\nu'}+W_{\nu\nu'}$ forms an 8×8 matrix which is given in Appendix A. For the SL structure, as the envelope function takes the form of $\psi=e^{iqz}\varphi(z)$, where $\varphi(z)=\varphi(z+d)$ with SL period d, the effective-mass equation for [111] SL can be constructed by replacing k'_z by $q-i\partial_{z'}$. The equations for the non-strained $\mathbf{k}\cdot\mathbf{p}$ formalism are given by

$$A=\mathsf{E}^{0}_{c}+\bar{\gamma}_c k_{t'}^2+V_c+\bar{\gamma}_c\left(q^2-i2q\partial_{z'}-\partial_{z'}^2\right), \tag{5}$$

$$S=\bar{P}_0\left(\frac{\omega^-}{2\sqrt{3}}k_{x'}-\frac{\omega^+}{6}k_{y'}\right)-\frac{\omega^+}{2\sqrt{3}}\bar{P}_0\left(q-i\partial_{z'}\right)=T,$$

$$C=-\frac{\sqrt{2}}{3}\bar{P}_0k_{y'}+\frac{1}{3}\bar{P}_0\left(q-i\partial_{z'}\right),$$

$$D=\sqrt{2}\bar{\gamma}_2\left(k_{x'}^2-k_{y'}^2\right)+4\bar{\gamma}_2k_{y'}\left(q-i\partial_{z'}\right),$$

$$F=\mathsf{E}^{0}_{v}-\bar{\gamma}^+k_{x'}^2-\bar{\gamma}^-k_{y'}^2-V_v-2\sqrt{2}\bar{\gamma}_2k_{y'}\left(q-i\partial_{z'}\right)-\bar{\gamma}_1\left(q^2-i2q\partial_{z'}-\partial_{z'}^2\right),$$

$$G=\mathsf{E}^{0}_{v}-\bar{\gamma}^-k_{x'}^2-\bar{\gamma}^+k_{y'}^2-V_v+2\sqrt{2}\bar{\gamma}_2k_{y'}\left(q-i\partial_{z'}\right)-\bar{\gamma}_1\left(q^2-i2q\partial_{z'}-\partial_{z'}^2\right),$$

$$H=\mathsf{E}_{s}-\bar{\gamma}_1k_{t'}^2-V_s-\bar{\gamma}_1\left(q^2-i2q\partial_{z'}-\partial_{z'}^2\right),$$

$$M = \bar{\gamma}_3\left(-2\omega^+ k_x k_{y'} + \frac{2\omega^-}{\sqrt{3}} k_{y'}^2\right) + \bar{\gamma}_3\left(\frac{\sqrt{2}\omega^-}{\sqrt{3}} k_{y'} + \sqrt{2}\omega^+ k_{x'}\right)\left(q - i\partial_{z'}\right) - \bar{\gamma}_3 \frac{2\omega^-}{\sqrt{3}}\left(q^2 - i2q\partial_{z'} - \partial_{z'}^2\right),$$

$$N = \bar{\gamma}_3(-i\sqrt{3}k_{x'}^2 + \frac{i}{\sqrt{3}}k_{y'}^2) + 2\bar{\gamma}_2 k_{x'} k_{y'} + \left(2\sqrt{2}\bar{\gamma}_2 k_{x'} + \frac{i2\sqrt{2}}{\sqrt{3}}\bar{\gamma}_3 k_{y'}\right)\left(q - i\partial_{z'}\right) + \frac{i2}{\sqrt{3}}\bar{\gamma}_3\left(q^2 - i2q\partial_{z'} - \partial_{z'}^2\right),$$

and equations from strained part are given by

$$\mathsf{A} = 3\bar{a}'\bar{e}_d ,$$

$$\mathsf{S} = -\frac{\omega^-}{2\sqrt{3}}\bar{P}_0\bar{e}' k_{x'} + \frac{\omega^+}{6}\bar{P}_0\bar{e}' k_{y'} + \frac{\omega^+}{3\sqrt{2}}\bar{P}_0\bar{\tilde{e}}\left(q - i\partial_{z'}\right) = \mathsf{T} ,$$

$$\mathsf{C} = \frac{\sqrt{2}}{3}\bar{P}_0\bar{e}' k_{y'} - \frac{1}{3}\bar{P}_0\bar{\tilde{e}}\left(q - i\partial_{z'}\right) ,$$

$$\mathsf{F} = \mathsf{G} = \mathsf{H} = -3\bar{a}\bar{e}_d ,$$

$$\mathsf{N} = -i\bar{d}\bar{e}_s ,$$

$$\mathsf{M} = \omega^-\bar{d}\bar{e}_s . \tag{6}$$

In the above we ignore the band and strain parameters B and b' in Eqs. (A4) and (A5), respectively, as these are small for the material system considered here [13]. The bar placed on top of the quantities in Eqs. (5) and (6) implies that these quantities include the "correction" part resulting from the difference in the band and strain parameters between materials A and B: e.g.,

$$\bar{\gamma}_c = \gamma_c^A + \theta_{z'}^B \Delta_{\gamma_c} , \tag{7}$$

where $\theta_{z'}^B = 1$ only in the material B region.

III. VARIATIONAL PROCEDURE

A variational form in the envelope-function representation for the present problem can be established as [38]

$$\begin{aligned}\mathsf{E}\sum_{l'} a_{l'}\int_{L_A+L_B} dz e^{-i2\pi(l-l')z/d} &= \sum_{l'} a_{l'}\left[\int_{L_A} dz e^{-i2\pi lz/d} H_A e^{i2\pi l'z/d} + \int_{L_B} dz e^{-i2\pi lz/d} H_B e^{i2\pi l'z/d}\right] \\ &+ \sum_{l'} a_{l'}\left[e^{-i2\pi lz/d} J_z^A e^{i2\pi l'z/d} - e^{-i2\pi lz/d} J_z^B e^{i2\pi l'z/d}\right]_{z=z_0} ,\end{aligned} \tag{8}$$

where $a_{l'}$ is the expansion coefficient to expand the envelope functions by sets of plane waves, $L_{A(B)}$ is the region of material A (B) along the z-direction and z_0 designates interface positions in z, and J_z^s is the current operator for material s.

If we define a unique envelope function over the entire SL structure; i.e., we expand the envelope functions in both material regions by the same kind of basis set, the envelope-function continuity condition makes these identical and makes current-continuity term disappeared. Note that the band-parameter difference is transformed into an SL potential in layer B so that the current-continuity is implicitly satisfied. This can be further simplified through "symmetrization " for indices l and l'; thus the resultant variational equation becomes

$$\mathsf{E}\,\mathbf{a} = \left(\mathbf{H}_A + \mathbf{H}_B\right)\mathbf{a} \equiv (\mathbf{H}_A^{total} + \mathbf{W})\mathbf{a} , \tag{9}$$

where

$$\mathbf{H}_A + \mathbf{H}_B = \int_{L_A} dz e^{-i2\pi lz/d} H_A e^{i2\pi l'z/d} + \int_{L_B} dz e^{-i2\pi lz/d} H_B e^{i2\pi l'z/d} \quad ,$$

$$\mathbf{H}_A^{total} = \int_{L_A+L_B} dz e^{-i2\pi lz/d} H_A e^{i2\pi l'z/d} \quad , \quad \mathbf{W} = \int_{L_B} dz e^{-i2\pi lz/d} (H_B - H_A) e^{i2\pi l'z/d} \quad . \tag{10}$$

The periodic part of the envelope function $\varphi(z)$ can be expanded by the Fourier series of plane waves $\exp(i2\pi lz/d)$, where l are integers. Operating the Hamiltonian on the plane waves can be achieved easily by replacing

$$\partial_z \to i\frac{2\pi l'}{d} \text{ or } k_{z'} \to q + 2\pi l'/d \ . \tag{11}$$

Thus the variational eigenvalue matrix $\mathbf{H}_{ll'}$, where

$$\mathbf{H}_{ll'} \equiv \frac{1}{d}\int_{-d/2}^{d/2} e^{-i2\pi lzld} \mathbf{H} e^{i2\pi l'z/d} \ , \tag{12}$$

consists of

$$A_{ll'} \equiv \frac{1}{d}\int_{-d/2}^{+d/2} dz e^{-i2\pi lz/d} A e^{i2\pi l'z/d} = \left\{\gamma_c\left[\left(q+\frac{2\pi l}{d}\right)^2 + k_{t'}^2\right] + \mathsf{E}_{c,0} + f_{l,l}^A\right\}\delta_{ll'} + f_{l,l'}^A \tilde{\delta}_{ll'} \ ,$$

$$S_{ll'} = T_{ll'} = \left[P_0\left(\frac{\omega^-}{2\sqrt{3}}k_{x'} - \frac{\omega^+}{6}k_{y'}\right) - \frac{\omega^+}{3\sqrt{2}}P_0\left(q+\frac{2\pi l}{d}\right) + f_{l,l}^S\right]\delta_{ll'} + f_{l,l'}^S\tilde{\delta}_{ll'} \ ,$$

$$C_{ll'} = \left\{P_0\left[-\frac{\sqrt{2}}{3}k_{y'} + \frac{1}{3}\left(q+\frac{2\pi l}{d}\right)\right] + f_{l,l}^C\right\}\delta_{ll'} + f_{l,l'}^C\tilde{\delta}_{ll'} \ ,$$

$$D_{ll'} = \left[\sqrt{2}\gamma_2\left(k_{x'}^2 - k_{y'}^2\right) + 4\gamma_2 k_{y'}\left(q+\frac{2\pi l}{d}\right) + f_{l,l}^D\right]\delta_{ll'} + f_{l,l'}^D\tilde{\delta}_{ll'} \ ,$$

$$F_{ll'} = -\left\{\gamma^+ k_{x'}^2 + \gamma^- k_{y'}^2 + 2\sqrt{2}\gamma_2 k_{y'}\left(q+\frac{2\pi l}{d}\right) + \gamma_1\left(q+\frac{2\pi l}{d}\right)^2 + f_{l,l}^F\right\}\delta_{ll'} - f_{l,l'}^F\tilde{\delta}_{ll'} \ ,$$

$$G_{ll'} = -\left\{\gamma^- k_{x'}^2 + \gamma^+ k_{y'}^2 + 2\sqrt{2}\gamma_2 k_{y'}\left(q+\frac{2\pi l}{d}\right) + \gamma_1\left(q+\frac{2\pi l}{d}\right)^2 + f_{l,l}^G\right\}\delta_{ll'} - f_{l,l'}^G\tilde{\delta}_{ll'} \ ,$$

$$H_{ll'} = -\left\{\mathsf{E}_{s,0} + \gamma_1\left[k_{x'}^2 + k_{y'}^2 + \left(q+\frac{2\pi l}{d}\right)^2\right] + f_{l,l}^H\right\}\delta_{ll'} - f_{l,l'}^H\tilde{\delta}_{ll'} \ ,$$

$$M_{ll'} = \left[-2\omega^+\gamma_3 k_{x'}k_{y'} + \frac{2\omega^-}{\sqrt{3}}k_{y'}^2 + \gamma_3\left(\frac{\sqrt{2}\omega^-}{\sqrt{3}}k_{y'} + \sqrt{2}\omega^+ k_{x'}\right)\left(q+\frac{2\pi l}{d}\right) - \frac{\sqrt{2}\omega^-}{\sqrt{3}}\gamma_3\left(q+\frac{2\pi l}{d}\right)^2 + f_{l,l}^Q\right]\delta_{ll'} + f_{l,l'}^Q\tilde{\delta}_{ll'} \ ,$$

$$N_{ll'} = \left[-i\sqrt{3}\gamma_3 k_{x'}^2 + i\frac{1}{\sqrt{3}}\gamma_3 k_{y'}^2 + 2\gamma_2 k_{x'}k_{y'} + \left(2\sqrt{2}\gamma_2 k_{x'} + i\frac{2\sqrt{2}}{\sqrt{3}}\gamma_3 k_{y'}\right)\left(q+\frac{2\pi l}{d}\right) + i\frac{2}{\sqrt{3}}\gamma_3\left(q+\frac{2\pi l}{d}\right)^2 + f_{l,l}^N\right]\delta_{ll'} + f_{l,l'}^N\tilde{\delta}_{ll'} \ , \tag{13}$$

and

$$\mathsf{A}_{ll'} = \left[3a'e_d + f^{\mathsf{A}}_{l,l}\right]\delta_{ll'} + f^{\mathsf{A}}_{l,l'}\tilde{\delta}_{ll'} ,$$

$$\mathsf{S}_{ll'} = \mathsf{T}_{ll'} = \left[P_0 e'\left(-\frac{\omega^-}{2\sqrt{3}}k_{x'} + \tfrac{\omega^+}{6}k_{y'}\right) + \frac{\omega^+}{3\sqrt{2}}P_0\tilde{e}\left(q + \frac{2\pi l}{d}\right) + f^{\mathsf{S}}_{l,l}\right]\delta_{ll'} + f^{\mathsf{S}}_{l,l'}\tilde{\delta}_{ll'} ,$$

$$\mathsf{C}_{ll'} = \left[\frac{\sqrt{2}}{3}P_0 e' k_{y'} - \frac{1}{3}P_0\tilde{e}\left(q + \frac{2\pi l}{d}\right) + f^{\mathsf{C}}_{l,l}\right]\delta_{ll'} + f^{\mathsf{C}}_{l,l'}\tilde{\delta}_{ll'} ,$$

$$\mathsf{D}_{ll'} = 0 ,$$

$$\mathsf{F}_{ll'} = \mathsf{G}_{ll'} = \mathsf{H}_{ll'} = -\left\{3ae_d + f^{\mathsf{F}}_{l,l}\right\}\delta_{ll'} - f^{\mathsf{F}}_{l,l'}\tilde{\delta}_{ll'} ,$$

$$\mathsf{M}_{ll'} = \left[\omega^- de_s + f^{\mathsf{M}}_{l,l}\right]\delta_{ll'} + f^{\mathsf{M}}_{l,l'}\tilde{\delta}_{ll'} ,$$

$$\mathsf{N}_{ll'} = -i\left[de_s + f^{\mathsf{N}}_{l,l}\right]\delta_{ll'} - if^{\mathsf{N}}_{l,l'}\tilde{\delta}_{ll'} . \tag{14}$$

The Fourier transformed potentials $f_{ll'}$ are given in Appendix B.

IV. HARTREE POTENTIALS

We start with the Poisson's equation

$$\nabla(\varepsilon_s \nabla U) = -\rho , \tag{15}$$

where

$$\rho = |q|(p - n + N_D^+ - N_A^-) . \tag{16}$$

Solving the equation by performing the integration from $-d/2$ to z gives

$$\varepsilon_s \nabla U(z) = \varepsilon_s \nabla U(-d/2) - \int_{-d/2}^{z} \rho(z')dz' . \tag{17}$$

Plugging $z = -d/2$ and $z = +d/2$, respectively, into Eq. (17) gives

$$\varepsilon_s \nabla U(-d/2) = \varepsilon_s \nabla U(-d/2) - \int_{-d/2}^{-d/2} \rho(z')dz' = \varepsilon_s \nabla U(-d/2) , \tag{18}$$

$$\varepsilon_s \nabla U(+d/2) = \varepsilon_s \nabla U(-d/2) - \int_{-d/2}^{+d/2} \rho(z')dz' = \varepsilon_s \nabla U(-d/2) . \tag{19}$$

This gives a boundary condition of

$$\nabla U(+d/2) = \nabla U(-d/2) . \tag{20}$$

Here we used the charge conservation condition of

$$\int_{-d/2}^{d/2} \rho(z')dz' = 0 . \tag{21}$$

Note that for a symmetric superlattice about a center along the z-direction, Eq. (20) becomes

$$\nabla U(+d/2) = \nabla U(-d/2) = 0. \tag{22}$$

Performing integration once again on Eq. (17) from $-d/2$ to z gives

$$U(z) = U(-d/2) + [\nabla U(-d/2)](z + d/2) - \int_{-d/2}^{z} \tfrac{1}{\varepsilon_s} dz' \int_{-d/2}^{z'} \rho(z'')dz'' . \tag{23}$$

For $z = +d/2$ it becomes

$$U(+d/2) = U(-d/2) + [\nabla U(-d/2)]d - \int_{-d/2}^{d/2} \tfrac{1}{\varepsilon_s} dz' \int_{-d/2}^{z'} \rho(z'')dz'' . \tag{24}$$

Since

$$U(+d/2) = U(-d/2) \tag{25}$$

due to the periodicity of SL, Eq. (24) gives an important boundary condition of

$$\nabla U(-d/2) = \frac{1}{d} \int_{-d/2}^{d/2} \tfrac{1}{\varepsilon_s} dz' \int_{-d/2}^{z'} \rho(z'')dz'' = \nabla U(+d/2) . \tag{26}$$

This can be simplified when we assume that ε_s is constant:

$$\nabla U(-d/2) = -\frac{1}{d\varepsilon_s} \int_{-d/2}^{d/2} z'\rho(z')dz' = \nabla U(+d/2) . \tag{27}$$

Equations (22), (25), and (26) consist of the necessary boundary conditions, which are summarized as

$$U(+d/2) = U(-d/2) ,$$

$$\nabla U(+d/2) = \nabla U(-d/2) = \frac{1}{d} \int_{-d/2}^{d/2} \tfrac{1}{\varepsilon_s} dz' \int_{-d/2}^{z'} \rho(z'')dz'' ,$$

or for constant ε_s

$$\nabla U(+d/2) = \nabla U(-d/2) = -\frac{1}{d\varepsilon_s} \int_{-d/2}^{d/2} z'\rho(z')dz' .$$

Incorporating Eq. (26) into Eq. (23) gives

$$U(z) = U(-d/2) + \left[\int_{-d/2}^{d/2} \tfrac{1}{\varepsilon_s} dz' \int_{-d/2}^{z'} \rho(z'')dz'' \right] \left(\frac{z + d/2}{d} \right) - \int_{-d/2}^{z} \tfrac{1}{\varepsilon_s} dz' \int_{-d/2}^{z'} \rho(z'')dz'' , \tag{28}$$

or for constant ε_s

$$U(z) = U(-d/2) - \left[\frac{1}{\varepsilon_s} \int_{-d/2}^{d/2} z'\rho(z')dz' \right] \left(\frac{z + d/2}{d} \right) - \frac{1}{\varepsilon_s} \int_{-d/2}^{z} (z - z')\rho(z')dz' . \tag{29}$$

Note that although $U(0) \neq 0$ in general, we can choose $U(0) = 0$ as a reference potential level in the computations.

V. EXCHANGE-CORRELATION POTENTIAL

The renormalization of the band gap in semiconductors due to high carrier densities has been studied in bulk systems over many years. It has been reported that under high optical excitation the band gap decreases with increasing carrier densities due to exchange-correlation effects in the electron-hole plasma.

Calculations of band gap renormalization for two-dimensional systems have been reported using both the Random Phase Approximation (RPA) [41] and the Local Density Approximation (LDA) [42]. The RPA self-energy is simply the energy of an electron interacting with itself via the RPA screened Coulomb interaction. The LDA gives a useful and simple description of these interactions in the ground state of many-body systems. Its applicability in QW systems with their spatially varying densities is not very clear, but it has been reported that it gives results in reasonable agreement with experimental results [41].

It has been experimentally found that the renormalization in a QW depends on the subbands involved in the transition. The strong subband dependence of this contribution stems from its dependence on the filling of the subbands through the Fermi occupation functions. The temperature dependence of the renormalization can be explained by the relative occupation of subband levels. For increasing temperatures the occupation of higher subbands increases, and therefore the renormalization of these subbands increases. On the other hand, for any constant total density the fraction of carriers occupying the lowest subband decreases if the temperature is raised. Both of these effects decrease the density difference between the first and second subbands and therefore decrease the dependence of band-gap renormalization on subbands, in agreement with experiment. Thus, for 300 K, for example, it may be acceptable to assume that all the subbands have a similar renormalization.

The comparisons of LDA results with the RPA results show that both provide the subband dependence of the renormalization somewhat less than that seen experimentally. The overall magnitude of the renormalization and the subband dependence of it, respectively, obtained from the LDA are smaller than those from the RPA. However, it has been shown that the LDA provides a reasonable, simple description of subband dependence of the band-gap shifts and that the overall magnitude of the renormalization is in reasonable agreement with experiment.

The LDA has been applied widely to study inhomogeneous one-component electronic systems, such as surfaces, impurities in metals, and atoms [43]. In it, the form of the full non-local exchange-correlation energy is replaced by that for a homogeneous system, and an approximate local form obtained from bulk results is used for it. It is known in homogeneous bulk systems that the sum of exchange and correlation energies for a system of equal densities of electrons and holes is to a good approximation independent of material and of band structure provided that the units of length and energy are given by the set of excitonic units appropriate for each material [44]. Furthermore, in such systems the magnitude of electron and hole self energies due to exchange and correlation effects have been found to be to a reasonable approximation equal and independent of wavevector [45].

For application of LDA to the two-component electron-hole system in QW structures, the total of the exchange-correlation energy is divided equally between electrons and holes: [42]

$$\mathsf{E}_{xc}[n_e(\mathbf{r}), n_h(\mathbf{r})] = (1/2)\int \left[n_e(\mathbf{r})\mathsf{E}_{xc}^{eh}\left(n_e(\mathbf{r})\right) + n_h(\mathbf{r})\mathsf{E}_{xc}^{eh}\left(n_h(\mathbf{r})\right)\right] d\mathrm{r}, \tag{30}$$

where E_{xc}^{eh} is the exchange-correlation energy per electron-hole pair. For the density dependence of the exchange-correlation effects, the same form suggested by Hedin and Lundqvist [43] for one-component systems has been used for both electrons and holes:

$$v_{xc}(r_s) = -[1 + B(r_s / A)\ln(1 + (A / r_s))][2 / \pi\alpha r_s)], \tag{31}$$

where $\alpha = (4/9\pi)^{1/3}$ and the parameters A and B are $A = 21$ and $B = 1.8913$, r_s is defined in the usual way for each component $(r_s)^3 = 3/4\pi a_0^3 n$, $a_0 = (\varepsilon_s / m_p)a_B$, ε_s static relative dielectric constant, a_B Bohr radius, and the mass is the optical mass [42] $m_p^{-1} = m_e^{-1} + m_h^{-1}$, where m_e and m_h are the electron and hole effective masses.

In the present work we make a slightly different generalization to the two-component electron and hole system, but in the same line of the method as above. Instead of the optical mass of m_p, we independently use Eq. (31) for the electrons and holes by using m_e and m_h, respectively, but with different fitting parameter *B*. The value of *B* turns out to be 0.7 which is the same as the original value given by Hedin and Lundqvist [43]. More quantitative analysis on the validity of this approximation should be made, but the results are found to maintain the same level of quality as those from the previous LDA [42] in terms of overall band-gap renormalization.

VI. OPTICAL MATRIX ELEMENT

In the dipole approximation, which is appropriate in practical QW structures, the momentum matrix element between the states, $|\mathbf{k}_t, n, q\rangle$ and $|\mathbf{k}_t, n, q\rangle$, is given by

$$\langle \mathbf{k}_t, n, q | \hat{\varepsilon}\cdot\mathbf{p} | \mathbf{k}_t, n', q \rangle \equiv \hat{\varepsilon}\cdot\mathbf{p}_{\mathrm{nn}'}(\mathbf{k}_t, q), \tag{32}$$

where **p** is the momentum operator, $\hat{\varepsilon}$ is the polarization unit vector of light, and direct transitions are assumed (i.e. transitions in which $\mathbf{k}_t$ and q are conserved). Upon substituting the SL state into this form, the matrix element may be conveniently described by utilizing the $D^{ij}_{\nu\nu'}$ notation [39], [46]:

$$\frac{\hbar}{m_0}\hat{\varepsilon}\cdot\mathbf{p}_{\mathrm{nn}'} \cong \sum_{\nu,\nu'}\Big\{ \Big[\int dz\psi(\nu,\mathbf{k}_t,n,q;z)*\psi(\nu',\mathbf{k}_t,n',q;z) \Big]\times\Big[\sum_i \varepsilon_i\big((D^{ix}_{\nu\nu'}+D^{xi}_{\nu\nu'})k_x+(D^{iy}_{\nu\nu'}+D^{yi}_{\nu\nu'})k_y\big) \Big]$$
$$+\Big[\int dz\psi(\nu,\mathbf{k}_t,n,q;z)*(-i\partial_z)\psi(\nu',\mathbf{k}_t,n',q;z) \Big]\times\Big[\sum_i \varepsilon_i\big(D^{iz}_{\nu\nu'}+D^{zi}_{\nu\nu'}\big) \Big] \Big\}. \tag{33}$$

with $i = x, y, z$.

Assuming the band constant $B = 0$ for the reason mentioned before, the optical matrix elements can be written in the same matrix structure as Eq. (A1):

$$A = (2\gamma_c k_{x'}Q)\hat{\varepsilon}_{x'} + (2\gamma_c k_{y'}Q)\hat{\varepsilon}_{y'} + (2\gamma_c R)\hat{\varepsilon}_{z'} ,$$

$$S = \left(\frac{\omega^-}{2\sqrt{3}}P_0Q\right)\hat{\varepsilon}_{x'} - \left(\frac{\omega^+}{6}P_0Q\right)\hat{\varepsilon}_{y'} - \left(\frac{\omega^+}{3\sqrt{2}}P_0Q\right)\hat{\varepsilon}_{z'} ,$$

$$T = \left(\frac{\omega^-}{2\sqrt{3}}P_0Q\right)\hat{\varepsilon}_{x'} - \left(\frac{\omega^+}{6}P_0Q\right)\hat{\varepsilon}_{y'} - \left(\frac{\omega^+}{3\sqrt{2}}P_0Q\right)\hat{\varepsilon}_{z'} ,$$

$$C = -\left(\frac{\sqrt{2}}{3}P_0Q\right)\hat{\varepsilon}_{y'} + \left(\frac{1}{3}P_0Q\right)\hat{\varepsilon}_{z'} ,$$

$$D = 2\sqrt{2}\gamma_2 k_{x'}Q\hat{\varepsilon}_{x'} + \left(-2\sqrt{2}\gamma_2 k_{y'}Q + 4\gamma_2 R\right)\hat{\varepsilon}_{y'} + 4\gamma_2 k_{y'}Q\hat{\varepsilon}_{z'} ,$$

$$F = -2\gamma^+ k_{x'}Q\hat{\varepsilon}_{x'} - \left(2\gamma^- k_{y'}Q + 2\sqrt{2}\gamma_2 R\right)\hat{\varepsilon}_{y'} - \left(2\sqrt{2}\gamma_2 k_{y'}Q + 2\gamma_1 R\right)\hat{\varepsilon}_{z'} ,$$

$$G = -2\gamma^- k_{x'}Q\hat{\varepsilon}_{x'} + \left(2\sqrt{2}\gamma_2 R - 2\gamma^+ k_{y'}Q\right)\hat{\varepsilon}_{y'} + \left(2\sqrt{2}\gamma_2 k_{y'}Q - 2\gamma_1 R\right)\hat{\varepsilon}_{z'} ,$$

$$H = -2\gamma_1 k_{x'}Q\varepsilon_{x'} - 2\gamma_1 k_{y'}Q\varepsilon_{y'} - 2\gamma_1 R\varepsilon_{z'} ,$$

$$M = \gamma_3\left(\sqrt{2}\omega^+ R - 2\omega^+ k_{y'}Q\right)\hat{\varepsilon}_{x'} + \gamma_3\left(-2\omega^+ k_{x'}Q + \frac{4\omega^-}{\sqrt{3}}k_{y'}Q + \frac{\sqrt{2}\omega^-}{\sqrt{3}}R\right)\hat{\varepsilon}_{y'} + \gamma_3\left(\sqrt{2}\omega^+ k_{x'}Q + \frac{\sqrt{2}\omega^-}{\sqrt{3}}k_{y'}Q - \frac{4\omega^-}{\sqrt{3}}R\right)\hat{\varepsilon}_{z'} ,$$

$$N = \left(-i2\sqrt{3}\gamma_3 k_{x'}Q + 2\gamma_2 k_{y'}Q + 2\sqrt{2}\gamma_2 R\right)\varepsilon_{x'} + \left(2\gamma_2 k_{x'}Q + \frac{i2}{\sqrt{3}}\gamma_3 k_{y'}Q + \frac{i2\sqrt{2}}{\sqrt{3}}\gamma_3 R\right)\varepsilon_{y'} ,$$
$$+\left(2\sqrt{2}\gamma_2 k_{x'}Q + \frac{i2\sqrt{2}}{\sqrt{3}}\gamma_3 k_{y'}Q + \frac{i4}{\sqrt{3}}\gamma_3 R\right)\varepsilon_{z'} , \tag{34}$$

where $\hat{\varepsilon}_i$, $i = x', y', z'$, is the unit polarization vector of light, and within the dipole approximation, the direct and dipole coupling coefficients of Q and R, respectively, for optical transitions from subband n to n' are defined as

$$Q^{nn'}_{\nu,\nu'} = \int dz\psi(\nu,\mathbf{k}_t,n,q;z)*\psi(\nu',\mathbf{k}_t,n',q;z) ,$$

$$R^{nn'}_{\nu,\nu'} = \int dz\psi(\nu,\mathbf{k}_t,n,q;z)*(-i\partial_z)\psi(\nu',\mathbf{k}_t,n',q;z) . \tag{35}$$

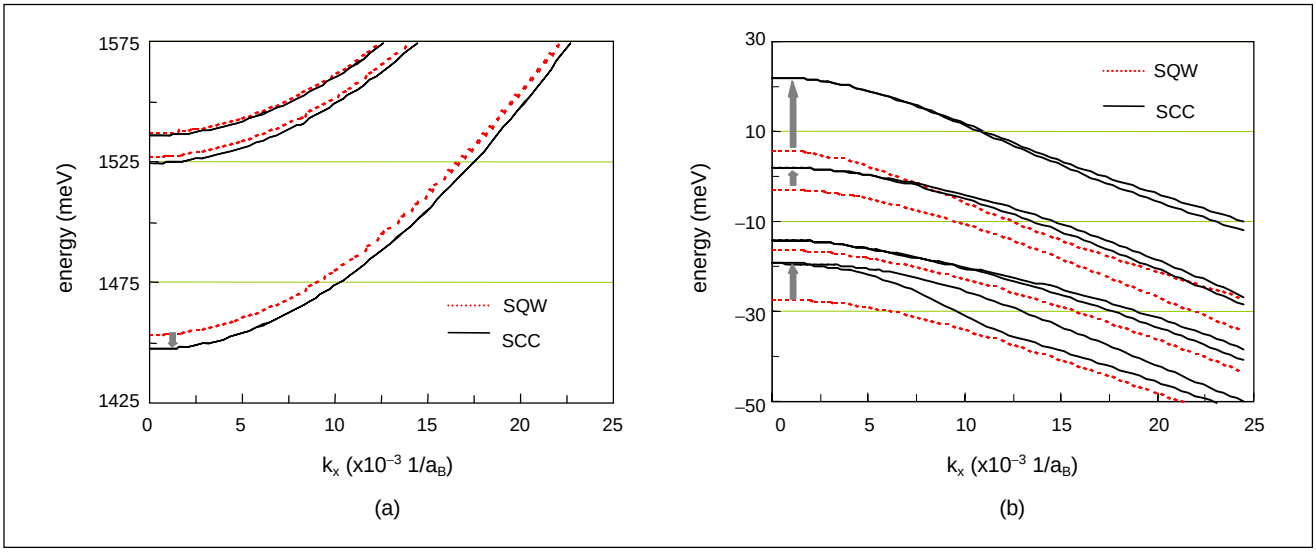

Fig. 1. Subband energy structure in the (a) conduction band and (b) valence band in terms of inplane wave vector. The inplane wave vector is taken along the x-direction. The solid lines are obtained from the self-consistent computation where the Hartree and exchange-correlation potentials and the piezoelectric field are taken into account (designated by "SCC"). The dotted lines are obtained without these factors (designated by "SQW"). Zero of the energy is taken at the top of the bulk valence band of InGaAs.

VII. SPONTANEOUS EMISSION RATE

Within the dipole approximation, the spontaneous emission rate of the intersubband transition from subband n to n' can be expressed as [47]

$$L_{nn'}(\hbar\omega) = \frac{\pi e^2 \hbar\omega}{m_0^2 \omega \varepsilon_s c' \Omega} \sum_{\mathbf{k}_t, q} \left| \hat{\varepsilon} \cdot \mathbf{p}_{nn'}(\mathbf{k}_t, q) \right|^2 f_n(\mathbf{k}_t, q)[1 - f_{n'}(\mathbf{k}_t, q)]$$

$$\times \frac{\hbar\Gamma_{nn'}}{(\mathrm{E}_{n'} - \mathrm{E}_n - \hbar\omega)^2 + (\hbar\Gamma_{nn'})^2}, \qquad (36)$$

where ε_s, c', Ω and f_n are, respectively, the dielectric constant, the speed of light in the material, the volume of the solid, and the Fermi distribution function. $\Gamma_{nn'}(\mathbf{k}_t, q)$ is the linewidth of the transition from n to n' for the state $(\mathbf{k}_t, q)$, which accounts for lifetime broadening due to scattering and inhomogeneity of well widths. In this paper $\hbar\Gamma_{nn'} = 5$ meV is assumed for numerical computations.

VIII. NUMERICAL COMPUTATIONS

For numerical computations, we take an [111] $In_{0.12}Ga_{0.88}As$/GaAs SL with 100 Å/100 Å well/barrier widths and compare the result with that obtained experimentally by Chin and Lin [25]. The pumped carrier density is assumed to be 1×10^{17} cm^{-3} over 40 Å width in the wells. The material parameters used in the calculations are summarized in Table 1. The ratio of band offsets between the conduction and valence bands is taken to be 25 % : 75 %. For 12 % of In, the piezoelectric field in the well is evaluated to be 52 KV/cm. The envelope-function equation of Eq. (1) is solved variationally, as shown in Eq. (8), by expanding envelope functions in terms of 33 orthogonal sets, which are chosen as periodic plane waves $\exp(i2\pi lz/d)$, where l and d are an integer and the SL period, respectively. Energies and envelope functions are obtained by

Table 1. Band and material parameters. All values for bulk GaAs and InAs are from Ref. [48]. All values for GaInAs are obtained by an interpolation.

Parameters	GaAs	InAs	$Ga_{0.88}In_{0.12}As$
a_0 (Å)	5.6533	6.0584	5.70
E_g at 15 K (eV)	1.522	0.410	1.388
γ_1	6.85	20.4	8.48
γ_2	2.1	8.3	2.84
γ_3	2.9	9.1	3.64
C_{11} (10^{11}dyn/cm^2)	11.88	8.329	11.5
C_{12} (10^{11}dyn/cm^2)	5.38	4.526	5.27
C_{44} (10^{11}dyn/cm^2)	5.94	3.959	5.70
a_v (eV)	–1.16	–1.00	–1.14
b (eV)	–1.7	–1.8	–1.71
d (eV)	–4.55	–3.6	–4.44
e_{14} (C/m^2)	0.16	0.045	0.15

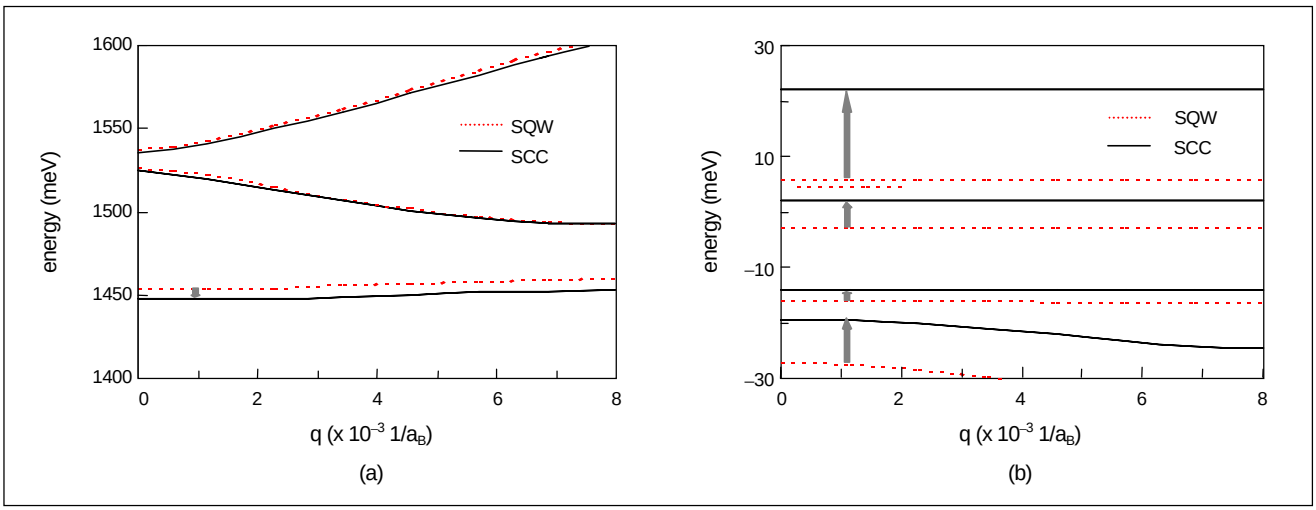

Fig. 2. Subband energy structure of (a) the conduction band and (b) valence band in terms of superlattice wave vector q. The solid lines are obtained from the self-consistent computation where the Hartree and exchange-correlation potentials and the piezoelectric field are taken into account (designated by "SCC"). The dotted lines are obtained without these factors (designated by "SQW").

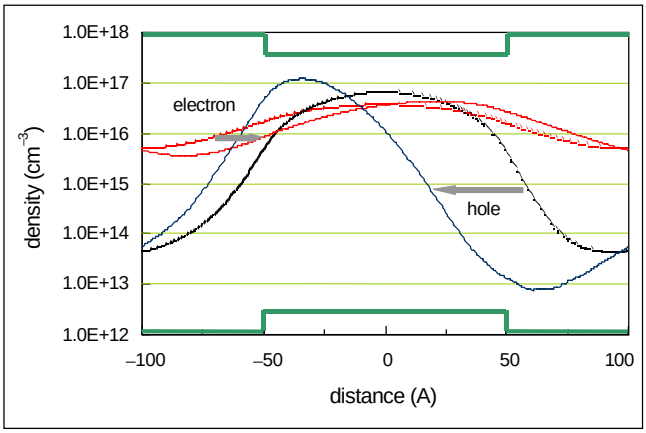

Fig. 3. Electron and hole distribution. The schematic picture of QW is inserted to provide a structural reference. The arrows designate change of distribution from the system ignoring the piezoelectric field to the one including the field. The pumped carrier density is assumed to be $1\times10^{17}\,\mathrm{cm}^{-3}$ over 40 Å width in the wells.

numerical diagonalization of $(8\times33)\times(8\times33)$ matrix for each quantum state (k_x, n, q), where the four conduction, heavy-hole, light-hole, and spin split-off bands are included in the primary band group.

Figures 1 and 2 show the $\mathrm{E}-k_x$ and $\mathrm{E}-q$ subband energies, respectively, with two types of computations. The solid lines are obtained from the self-consistent computation where the Hartree and exchange-correlation potentials and the piezoelectric field are taken into account (designated by "SCC" in the figure). The dotted lines are obtained without these factors (designated by "SQW" in the figure). The result shows a significant subband renormalization (about 23 meV reduction between CB1 and VB1). The renormalization becomes larger for the subband with heavier effective mass due to larger exchange-correlation potential. The figure also shows that the subband energies obtained from SCC become split as away from $k_x = 0$. This is due to removal of spatial symmetry along the growth direction by the piezoelectric field.

Figure 3 shows the change in the distribution of electrons and holes when the peizoelectric field is incorporated. The schematic picture of the QW is inserted as a structural reference. Initially both carriers are distributed symmetrically around the center of QW. The piezoelectric field separates electrons and holes in the opposite direction. This is more effective for holes as holes are spatially more confined due to heavier effective mass, and consequently produce more noticeable change with the electric field. This separation, in turn, results in significant change in optical transition matrix element and absorption and emission coefficients.

Figure 4 shows the optical momentum matrix elements (MME) of the lights polarized in the x-direction [Fig. 4(a)] and in the growth (z) direction [Fig. 4(b)]. For both polarizations, the MME of CB1-VB1 (MME between the lowest subband in CB and the highest subband in VB) significantly reduces as the piezoelectric field is included, while the MME of CB1-VB2 increases significantly. Note that for a symmetric QW structure the transition of CB1-VB2 is forbidden at the zone center due to the parity of envelope functions involved. The non-zero MME of CB1-VB2 at $k_x = 0$ and also the large increase in magnitude of MME demonstrate that the symmetry is broken. On the other hand, the reduction of MME for CB1-VB1 is mainly dueto the separation of electrons and holes.

Figure 5 shows the spontaneous emission rate between CB1 and VB1 for both polarizations of light. The emission result

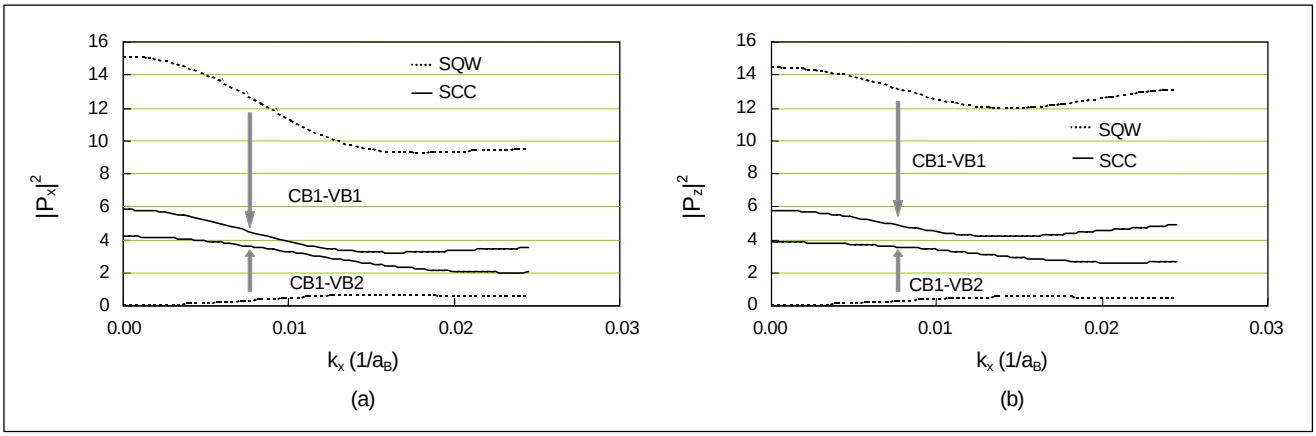

Fig. 4. Optical momentum matrix elements (MME) of the lights polarized (a) in the x-direction and (b) in the growth (z) direction. For both polarizations, the upper two lines are for CB1-VB1 transition and the lower two lines for CB1-VB2. The arrows designate change of MME when the piezoelectric field is included.

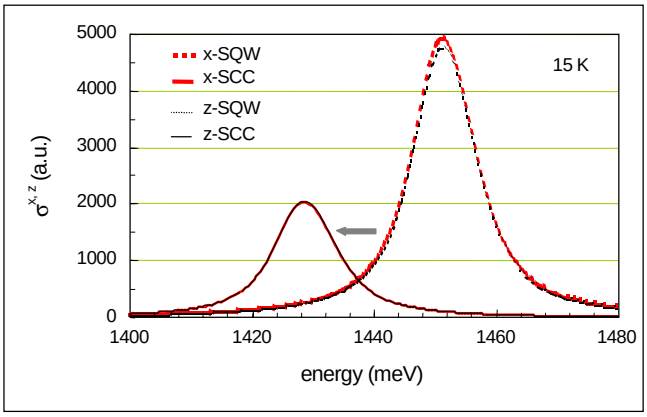

Fig. 5. Spontaneous emission rate between CB1 and VB1 for both x- and z-polarization of light. The temperature is assumed to be 15 K. The results with inclusion of piezoelectric field (SCC) appear to be almost identical for both polarizations of light.

without inclusion of the piezoelectric field has peak at 1451 meV, while that with the field at 1429 meV. The shift is mainly due to the bandgab renormalization, which is 23 meV at the center of subband, and a small Stark shift due to the electric field. The reduction of peak magnitude is due to the decrease in MME resulting from separation of the two types of carriers. The temperature is assumed to be 15 K in the computation. The temperature and the structural parameters are chosen to make a similar condition for comparison to the photoluminescence (PL) experiment by Chin and Lin [25]. Their PL peak was at around 1470 meV. Thus there is a 40 meV discrepancy between the two results. As mentioned earlier, the InGaAs parameters used in the computation were obtained by the linear interpolation between the parameters of bulk GaAs and InAs. In the computation, no adjustment of parameters has been conducted. Thus, it is expected that the difference between the theoretical and experimental results comes from the large uncertainty in the values of material parameters, especially in the band gap of InGaAs.

IX. CONCLUSIONS

We presented a calculation model for more quantitative theoretical analysis of electronic and optical properties of strained piezoelectric [111] InGaAs/GaAs superlattices (SLs). The model takes into account a full band-coupling between the four important bands of conduction, heavy, light, and spin split-off valence bands. In this model, the difference in bulk Bloch states and band parameters between constituent materials are transformed to be a SL potential in the larger band-gap material region, which, as a result, removes the interface-matching problem at the heterojunction interfaces.

The model self-consistently solves an 8×8 Schrödinger equation and equations of Hartree and exchange-correlation potentials using the variational procedure. It provides the subband energy structure and envelope functions, which in turn are used to calculate optical matrix elements and spontaneous emission rates.

The Poisson's equation has been reviewed for calculation of the Hartree potential for general, not symmetric QW systems, and relevant boundary conditions were derived. For taking into account the renormalization of the band gap due to high carrier densities, a slightly different calculation model of exchange-correlation potential has been presented for the two-component electron and hole system within the local density approximation.

As an illustration of application of the present model, and also to briefly investigate the effect of piezoelectric field on electronic and optical properties of the QW structure, numerical computations have been performed on a strain-induced piezoelectric [111] GaAs/InGaAs SL with well/barrier thicknesses of 100 Å/100 Å and 12 % of In mole fraction.

The comparison between the theoretical and experimental PL peaks for CB1-VB1 transition shows a large discrepancy amounting to 40 meV. The InGaAs parameters used in the present computations were obtained by a linear interpolation between values of bulk GaAs and InAs. In the computations, no adjustment of parameters has been conducted. Thus, it is expected that the difference between the theoretical and experimental results comes from the large uncertainty in the values of material parameters, especially the band gap of InGaAs.

Beside the discrepancy, however, the theoretical model successfully reveals all the important characteristics coming from appearance of the piezoelectric field. Among the various effects from the piezoelectric field, it has been shown that most significant consequences are the removal of spatial symmetry and separation of electrons and holes, which result in a large change in optical transition properties.

Thus, the model can be used to further elucidate the recent theoretical results and experimental observations of interesting properties of this type of quantum well (QW) and SL structures, including screening of piezoelectric field and its resultant optical nonlinearities, which have been intensively studied for use in the design of novel opto-electronic devices.

ACKNOWLEDGEMENT

The authors wish to acknowledge Dr. K. C. Park, Mr. S. R. Kang, and Dr. C. H. Yim in ETRI for supporting this work.

APPENDIX A

The structure of 8×8 matrix [40] for $H_{vv'}+W_{vv'}$ is given as

$$\begin{bmatrix} \mathrm{A} & 0 & -\mathrm{S} & 0 & -\sqrt{3}\mathrm{T}^* & -\sqrt{2}\mathrm{C} & -\mathrm{C} & -\sqrt{2}\mathrm{S} \\ 0 & \mathrm{A} & -\sqrt{2}\mathrm{C} & \sqrt{3}\mathrm{S} & 0 & \mathrm{T}^* & -\sqrt{2}\mathrm{T}^* & \mathrm{C} \\ -\mathrm{S}^* & -\sqrt{2}\mathrm{C}^* & \mathrm{G} & \mathrm{M}^* & \mathrm{N} & 0 & -\frac{\sqrt{3}}{\sqrt{2}}\mathrm{M} & -\mathrm{D} \\ 0 & \sqrt{3}\mathrm{S}^* & \mathrm{M} & \mathrm{F} & 0 & \mathrm{N} & -\sqrt{2}\mathrm{N} & -\frac{1}{\sqrt{2}}\mathrm{M} \\ -\sqrt{3}\mathrm{T} & 0 & \mathrm{N}^* & 0 & \mathrm{F} & -\mathrm{M}^* & -\frac{1}{\sqrt{2}}\mathrm{M}^* & \sqrt{2}\mathrm{N}^* \\ -\sqrt{2}\mathrm{C}^* & \mathrm{T} & 0 & \mathrm{N}^* & -\mathrm{M} & \mathrm{G} & \mathrm{D} & -\frac{\sqrt{3}}{\sqrt{2}}\mathrm{M}^* \\ -\mathrm{C}^* & -\sqrt{2}\mathrm{T} & -\frac{\sqrt{3}}{\sqrt{2}}\mathrm{M}^* & -\sqrt{2}\mathrm{N}^* & -\frac{1}{\sqrt{2}}\mathrm{M} & \mathrm{D} & \mathrm{H} & 0 \\ -\sqrt{2}\mathrm{S}^* & \mathrm{C}^* & -\mathrm{D} & -\frac{1}{\sqrt{2}}\mathrm{M}^* & \sqrt{2}\mathrm{N} & -\frac{\sqrt{3}}{\sqrt{2}}\mathrm{M} & 0 & \mathrm{H} \end{bmatrix}. \tag{A1}$$

The basis functions for this equation are chosen as

$$\mathrm{CB1}(\Gamma_6,1/2)=|S\rangle\uparrow\ ,$$

$$\mathrm{CB2}(\Gamma_6,-1/2)=|S\rangle\downarrow\ ,$$

$$\mathrm{HH1}(\Gamma_8,-1/2)=\frac{i}{\sqrt{2}}(|X'\rangle+i|Y'\rangle)\uparrow\ ,$$

$$\mathrm{HH2}(\Gamma_8,1/2)=\frac{-i}{\sqrt{2}}(|X'\rangle-i|Y'\rangle)\downarrow\ ,$$

$$\mathrm{LH1}(\Gamma_8,-3/2)=\frac{-i}{\sqrt{6}}(|X'\rangle+i|Y'\rangle)\downarrow+i\frac{\sqrt{2}}{\sqrt{3}}|Z'\rangle\uparrow\ ,$$

$$\mathrm{LH2}(\Gamma_8,3/2)=\frac{i}{\sqrt{6}}(|X'\rangle-i|Y'\rangle)\uparrow+i\frac{\sqrt{2}}{\sqrt{3}}|Z'\rangle\downarrow\ ,$$

$$\mathrm{SH1}(\Gamma_7,1/2)=\frac{-i}{\sqrt{3}}(|X'\rangle+i|Y'\rangle)\downarrow-\frac{i}{\sqrt{3}}|Z'\rangle\uparrow\ ,$$

$$\mathrm{SH2}(\Gamma_7,-1/2)=\frac{-i}{\sqrt{3}}(|X'\rangle-i|Y'\rangle)\uparrow+\frac{i}{\sqrt{3}}|Z'\rangle\downarrow\ , \tag{A2}$$

where the label Γ specifies the irreducible representation of the T_d double group; $|S\rangle$ represents the s-like spatial function, and $|X'\rangle$, $|Y'\rangle$, and $|Z'\rangle$ represent the p-like functions; and the arrows designate the two eigenspinors of the operator $\sigma_{z'}$:

$$\uparrow=\begin{pmatrix}1\\0\end{pmatrix}\text{ and }\downarrow=\begin{pmatrix}0\\1\end{pmatrix}. \tag{A3}$$

The primes in the basis functions indicate that these are transformed by an orthogonal rotation so that z' is aligned to the [111] direction.

Based on the above basis functions, the non-strained $\mathbf{k}\cdot\mathbf{p}$ part (represented by slant capital characters, e.g., A) and strain-interaction part (represented by script characters, e.g., $\mathcal{A}$) are, respectively, given as:

$$A=(\mathcal{E}_c+\gamma_c k_{t'}^2)+\gamma_c k_{z'}^2,$$

$$S=\left(\frac{P_0\omega^-}{2\sqrt{3}}k_{x'}-\frac{P_0\omega^+}{6}k_{y'}-\frac{B\omega^+}{3\sqrt{2}}k_{x'}k_{y'}+\frac{B\omega^-}{3\sqrt{6}}k_{y'}^2\right)-\left(\frac{B\omega^+}{3\sqrt{2}}-\frac{B\omega^-}{6\sqrt{3}}k_{y'}-\frac{B\omega^+}{6}k_{x'}\right)k_{z'}-\frac{B\omega^-}{3\sqrt{6}}k_{z'}^2\ ,$$

$$T=\left(\frac{P_0\omega^-}{2\sqrt{3}}k_{x'}-\frac{P_0\omega^+}{6}k_{y'}+\frac{B\omega^+}{3\sqrt{2}}k_{x'}k_{y'}-\frac{B\omega^-}{3\sqrt{6}}k_{y'}^2\right)-\left(\frac{P_0\omega^+}{3\sqrt{2}}+\frac{B\omega^-}{6\sqrt{3}}k_{y'}+\frac{B\omega^+}{6}k_{x'}\right)k_{z'}+\frac{B\omega^-}{3\sqrt{6}}k_{z'}^2\ ,$$

$$C=-\left(\frac{\sqrt{2}P_0}{3}k_{y'}-\frac{iB}{2\sqrt{3}}k_{x'}^2+\frac{iB}{3\sqrt{2}}k_{y'}^2\right)+\left(\frac{P_0}{3}-\frac{iB}{3\sqrt{6}}k_{y'}\right)k_{z'}-\frac{iB}{3\sqrt{3}}k_{z'}^2\ ,$$

$$D=\sqrt{2}\gamma_2(k_{x'}^2-k_{y'}^2)+(4\gamma_2 k_{y'})k_{z'},$$

$$F=-(\gamma^+k_{x'}^2+\gamma^-k_{y'}^2)-(2\sqrt{2}\gamma_2 k_{y'})k_{z'}-\gamma_1 k_{z'}^2,$$

$$G=-(\gamma^-k_{x'}^2+\gamma^+k_{y'}^2)+(2\sqrt{2}\gamma_2 k_{y'})k_{z'}-\gamma_1 k_{z'}^2,$$

$$H=-(\mathcal{E}_s+\gamma_1 k_{t'}^2)-\gamma_1 k_{z'}^2\ ,$$

$$M=\left(-2\omega^+\gamma_3 k_{x'}k_{y'}+\frac{2\omega^-\gamma_3}{\sqrt{3}}k_{y'}^2\right)+\left(\frac{\sqrt{2}\omega^-\gamma_3}{\sqrt{3}}k_{y'}+\sqrt{2}\omega^+\gamma_3 k_{x'}\right)k_{z'}-\frac{2\omega^-\gamma_3}{\sqrt{3}}k_{z'}^2,$$

$$N=\left(-i\sqrt{3}\gamma_3 k_{x'}^2+2\gamma_2 k_{x'}k_{y'}+\frac{i}{\sqrt{3}}\gamma_3 k_{y'}^2\right)+\left(2\sqrt{2}\gamma_2 k_{x'}+\frac{i2\sqrt{2}}{\sqrt{3}}\gamma_3 k_{y'}\right)k_{z'}+\frac{i2\gamma_3}{\sqrt{3}}k_{z'}^2, \tag{A4}$$

and

$$\mathsf{A} = 3a'e_d \ ,$$

$$\mathsf{S} = -\frac{b'\omega^-}{\sqrt{3}}e_s - \frac{P_0\omega^-}{2\sqrt{3}}e'k_{x'} + \frac{P_0\omega^+}{6}e'k_{y'} + \frac{P_0\omega^+}{3\sqrt{2}}\tilde{e}k_{z'} \ ,$$

$$\mathsf{M} = d\omega^- e_s \ ,$$

$$\mathsf{F} = \mathsf{G} = \mathsf{H} = -3ae_d \ ,$$

$$\mathsf{T} = \frac{\omega^-}{\sqrt{3}}b'e_s - \frac{\omega^-}{2\sqrt{3}}P_0e'k_{x'} + \frac{\omega^+}{6}P_0e'k_{y'} + \frac{\omega^+}{3\sqrt{2}}P_0\tilde{e}k_{z'} \ ,$$

$$\mathsf{C} = -i\frac{1}{\sqrt{3}}b'e_d + \frac{\sqrt{2}}{3}P_0e'k_{y'} - \frac{1}{3}P_0\tilde{e}k_{z'} \ ,$$

$$\mathsf{N} = -ide_s \ . \qquad \text{(A5)}$$

Here E_c and E_s are band edge energies of the conduction and spin split-off bands, respectively, and we set $\mathsf{E}_v \equiv 0$. The other quantities included in these equations are defined as

$$\omega^{\pm} = 1 \pm i \ ,$$

$$\gamma_c = A' + 1 \ ,$$

$$\gamma^{\pm} = \gamma_1 \pm \gamma_2 \ ,$$

$$P_0 = -i\frac{\hbar}{m_0}\langle s|p_x|\Gamma_4 j\rangle \ ,$$

$$A' = \frac{\hbar^2}{m_0^2}\sum_{nj}\frac{\left|\langle s|p_x|n\Gamma_4 j\rangle\right|^2}{\mathsf{E}_c - \mathsf{E}_{n\Gamma_4}} \ ,$$

$$B = 2\frac{\hbar^2}{m_0^2}\sum_{nj}\frac{\langle s|p_x|n\Gamma_4 j\rangle\langle n\Gamma_4 j|p_y|Z\rangle}{\mathsf{E}_c - \mathsf{E}_{n\Gamma_4}} \ , \qquad \text{(A6)}$$

where j labels the row to which the function associated with Γ belongs, and n specifies the band (in the summation the bottom of conduction band with energy of E_c is not included because this band is included in the primary band set), and

$$e_{xx} = e_{yy} = e_{zz} \equiv e_d \ ,$$

$$e_{xy} = e_{yz} = e_{zx} \equiv e_s \ ,$$

$$e' \equiv e_d - e_s \ ,$$

$$\tilde{e} \equiv e_d + 2e_s$$

$$a' = \langle s|D_{xx}|s\rangle \ ,$$

$$b' = 2\langle s|D_{xy}|z\rangle \ ,$$

$$d = \frac{2}{\sqrt{3}}\langle X|D_{xx}|Z\rangle \ . \qquad \text{(A7)}$$

In the above D_{xy} is the x, y component of the operator D_{ij} defined by writing D_0 as [40]

$$D_0 = \sum_{ij}\left[-\frac{1}{m_0}p_i p_j + V_{ij}\right]e_{ij} \qquad \text{(A8)}$$

and the strain constant e_{ij} can be found in the literature [4]. The modified Luttinger parameters are related to the original Luttinger parameters with superscript L by [40]

$$\gamma_1 = \gamma_1^L - \frac{\mathsf{E}_p}{3\mathsf{E}_g + \Delta} \ ,$$

$$\gamma_2 = \gamma_2^L - \frac{1}{2}\frac{\mathsf{E}_p}{3\mathsf{E}_g + \Delta} \text{, and}$$

$$\gamma_3 = \gamma_3^L - \frac{1}{2}\frac{\mathsf{E}_p}{3\mathsf{E}_g + \Delta} \ , \qquad \text{(A9)}$$

where E_g is the band gap between the conduction band (Γ_6) and the valence band (Γ_8), and

$$\mathsf{E}_p = \frac{2m_0}{\hbar^2}P_0^2 \ . \qquad \text{(A10)}$$

APPENDIX B

The Fourier transformed potentials $f_{ll'}$ included in Eqs. (13) and (14) are given by

$$f_{l,l'}^A = h_{l-l'}\left\{\Delta_{\gamma_c}\left[\ q + \frac{\pi(l+l')}{d}\ \right]^2 + \Delta_{\gamma_c}k_{l'}^2 + V_c\right\}, \qquad \text{(B1)}$$

$$f_{l,l'}^S = f_{l,l'}^T = h_{l-l'}\Delta_{P_0}\left\{\frac{\omega^-}{2\sqrt{3}}k_{x'} - \frac{\omega^+}{6}k_{y'} - \frac{\omega^+}{3\sqrt{2}}\left[\ q + \frac{\pi(l+l')}{d}\ \right]\right\},$$

$$f_{l,l'}^C = h_{l-l'}\Delta_{P_0}\left\{-\frac{\sqrt{2}}{3}k_{y'} + \frac{1}{3}\left[\ q + \frac{\pi(l+l')}{d}\ \right]\right\},$$

$$f_{l,l'}^{D} = h_{l-l'}\Delta_{\gamma_2}\left\{\sqrt{2}\left(k_{x'}^2 - k_{y'}^2\right) + 4k_{y'}\left[\ q + \frac{\pi(l+l')}{d}\ \right]\right\},$$

$$f_{l,l'}^{F} = h_{l-l'}\left\{\ \Delta_{\gamma^+}k_{x'}^2 + \Delta_{\gamma^-}k_{y'}^2 + 2\sqrt{2}\gamma_2 k_{y'}\left[\ q + \frac{\pi(l+l')}{d}\ \right] + \Delta_{\gamma_1}\left[\ q + \frac{\pi(l+l')}{d}\ \right]^2 + V_v\ \right\},$$

$$f_{l,l'}^{G} = h_{l-l'}\left\{\ \Delta_{\gamma^-}k_{x'}^2 + \Delta_{\gamma^+}k_{y'}^2 + 2\sqrt{2}\gamma_2 k_{y'}\left[\ q + \frac{\pi(l+l')}{d}\ \right] + \Delta_{\gamma_1}\left[\ q + \frac{\pi(l+l')}{d}\ \right]^2 + V_v\ \right\},$$

$$f_{l,l'}^{H} = h_{l-l'}\left\{\Delta_{\gamma_1}k_{l'}^2 + \Delta_{\gamma_1}\left[\ q + \frac{\pi(l+l')}{d}\ \right]^2 + V_s\right\},$$

$$f_{l,l'}^{M} = h_{l-l'}\Delta_{\gamma_3}\left\{-2\omega^+ k_{x'}k_{y'} + \frac{2\omega^-}{\sqrt{3}}k_{y'}^2 + \left(\ \frac{\sqrt{2}\omega^-}{\sqrt{3}}k_{y'} + \sqrt{2}\omega^+ k_{x'}\ \right)\left[\ q + \frac{\pi(l+l')}{d}\ \right] - \bar{\gamma}_3\frac{2\omega^-}{\sqrt{3}}\left[\ q + \frac{\pi(l+l')}{d}\ \right]^2\right\},$$

$$f_{l,l'}^{N} = h_{l-l'}\left\{\Delta_{\gamma_3}\left(\ -i\sqrt{3}k_{x'}^2 + i\frac{1}{\sqrt{3}}k_{y'}^2\ \right) + 2\gamma_2 k_{x'}k_{y'} + \left(\ 2\sqrt{2}\Delta_{\gamma_2}k_{x'} + i\frac{2\sqrt{2}}{\sqrt{3}}\Delta_{\gamma_3}k_{y'}\ \right)\left[\ q + \frac{\pi(l+l')}{d}\ \right]\right.$$
$$\left. + i\frac{2}{\sqrt{3}}\Delta_{\gamma_3}\left[\ q + \frac{\pi(l+l')}{d}\ \right]^2\right\},$$

and

$$f_{l,l'}^{\mathsf{A}} = h_{l-l'}\left[3(\Delta_{a'}e_d + a'\Delta_{e_d})\right], \tag{B2}$$

$$f_{l,l'}^{\mathsf{S}} = f_{l,l'}^{\mathsf{T}} = h_{l-l'}\left\{\Delta_{P_0}\left[\ -\frac{\omega^-}{2\sqrt{3}}e'k_{x'} + \frac{\omega^+}{6}e'k_{y'} + \frac{\omega^+}{3\sqrt{2}}\tilde{e}(q + \frac{2\pi l'}{d})\ \right] + P_0\left[\ -\frac{\omega^-}{2\sqrt{3}}\Delta_{e'}k_{x'} + \frac{\omega^+}{6}\Delta_{e'}k_{y'} + \frac{\omega^+}{3\sqrt{2}}\Delta_{\tilde{e}}(q + \frac{2\pi l'}{d})\ \right]\right\},$$

$$f_{l,l'}^{\mathsf{C}} = h_{l-l'}\left[\frac{\sqrt{2}}{3}(\Delta_{P_0}e' + \frac{\sqrt{2}}{3}P_0\Delta_{e'})k_{y'} + \frac{1}{3}(\Delta_{P_0}\tilde{e} + P_0\Delta_{\tilde{e}})(q + \frac{2\pi l'}{d})\right],$$

$$f_{l,l'}^{\mathsf{F}} = f_{l,l'}^{\mathsf{G}} = f_{l,l'}^{\mathsf{H}} = h_{l-l'}\left[3(\Delta_a e_d + a\Delta_{e_d})\right],$$

$$f_{l,l'}^{\mathsf{M}} = h_{l-l'}\omega^-(\Delta_d e_s + d\Delta_{e_s}),$$

$$f_{l,l'}^{\mathsf{N}} = h_{l-l'}(\Delta_d e_s + d\Delta_{e_s}),$$

where

$$h_{l-l'} = \frac{\cos[(l-l')\pi]\sin[(l-l')\pi b/d]}{(l-l')\pi}, \tag{B3}$$

with barrier thickness b. Note that the expansion indices l and l' are symmetrized, and for $l = l'$ Eq. (B3) is replaced by

$$h_{l-l'} \to \frac{b}{d}. \tag{B4}$$

REFERENCES

[1] D. L. Smith, "Strain-Generated Electric Fields in [111] Growth Axis Strained-Layer Superlattices," *Solid State Comm*. Vol. 57, 1986, p. 919.

[2] G. C. Osbourn, "Strained-Layer Superlattices from Lattice Mismatched Materials," *J. Appl. Phys.,* Vol. 53, 1982, p. 1586.

[3] E. S. Snow, B. V. Shanabrook, and D. Gammon, "Strain-Induced Two-Dimensional Electron Gas in [111] Growth-Axis Strained-Layer Structures," *Appl. Phys. Lett*. Vol. 56, 1990, p. 758.

[4] D. L. Smith and C. Mailhiot, "Theory of Semiconductor Superlattice Electronic Structure," *Review of Modern Physics,* Vol. 62, 1990, p. 173.

[5] T. Anan, K. Nishii, and S. Sugou, *Appl. Phys. Lett.,* Vol. 60, 1992, p. 3159.

[6] R. A. H. Hamilton and P. Rees, "Line Broadening due to Carrier-Carrier Scattering in Quantum Well Heterostructures," *Semicond. Sci. Technol.*, Vol. 8, 1993, p. 728.

[7] R. L. Tober and T. H. Bahder, "Determining the Electric Field in [111] Strained-Layer Quantum Wells," *Appl. Phys. Lett.,* Vol. 63, 1993, p. 2369.

[8] J. L. Sanchez-Rojas, A. Sacedon, F. Gonzalez-Sanz, E. Calleja, and E. Munoz, "Dependence on the In Concentration of the Piezoelectric Field in [111]B InGaAs/GaAs Strained Heterostructures," *Appl. Phys. Lett.,* Vol. 65, 1994, p. 2042.

[9] M. Livingstone, I. Galbraith, and B. S. Wherrett, "Comparison of Optical Nonlinearities in Piezoelectric Strained [111]- and [001]-Grown (In,Ga)As/(Al,Ga)As Quantum Wells," *Appl. Phys. Lett.,* Vol. 65, 1994, p. 2771.

[10] P. J. Rodriguez-Girones and G. J. Rees, "Electronic Structure and Field Screening Effects in 111 InGaAs-GaAs Strained Layer Piezoelectric Quantum-Wells," *IEEE Photonics Technology Letters*, Vol. 7, 1995, p. 71.

[11] X. Chen, C. H. Molloy, D. A. Woolf, C. Cooper, D. J. Somerford, P. Blood, K.A. Shore, and J. Sarma, "Piezoelectric Field Effects in InGaAs [111]B Quantum Wells," *Appl. Phys. Lett.,* Vol. 67, 1995, p. 1393.

[12] Toshihide Watanabe, Teiji Yamamoto, Pablo O. Vaccaro, Hajime Ohnishi, and Kazuhisa Fujita, "AlGaAs/GaAs and InGaAs/GaAs QWs Grown on GaAs [111]A Substrates," *Microelectronics Journal,* Vol. 27, 1996, p. 411.

[13] J. Los, A. Fasolino, and A. Catellani, "Generalization of the k.p Approach for Strained Semiconductor Structures Grown on High-Index-Planes," *Phys. Rev. B,* Vol. 53, 1996, p. 4630.

[14] H. G. Colson and D. J. Dunstan, "Equilibrium Critical Thickness of Epitaxial Strained Layers in the {111} Orientations," *J. Appl. Phys.,* Vol. 81, 1997, p. 2898.

[15] S. Picozzi, A. Continenza, and A. J. Freeman, "Electric Fields and Valence-Band Offsets at Strained [111] Heterostructures," *Phys. Rev. B,* Vol. 55, 1997, p. 13080.

[16] P. Ballet, P. Disseix, J. Leymarie, A. Vasson, A-M Vasson, and R. Grey, "Excitonic Properties in [111]B-Grown (In,Ga)As/GaAs Piezoelectric Multiple Quantum Wells," *Phys. Rev. B*, Vol. 56, 1997, p. 15202.

[17] M. Moran, K. J. Moore, and P. Dawson, "Barrier Thickness Dependence of the Photoscreening of the Piezoelectric Field in [111] Oriented GaAs-InxGa1-xAs Double Quantum Wells," *J. Appl. Phys.,* Vol. 84, 1998, p. 3349.

[18] John D. Bruno and Richard L. Tober, "Effects of the Piezoelectric Field on Quantum-Confined Stark Effect in [111]B InGaAs Quantum-Well Structure," *J. Appl. Phys.,* Vol. 85, 1999, p. 2221.

[19] T. Sauncy, M. Holtz, O. Brafman, D. Fekete, and Y. Finkelstein, "Exciton Intensity Dependence of PL from Narrow [100]- and [111]A-Grown InxGa1-xAs/GaAs QWs," *Phys. Rev. B,* Vol. 59, 1999, p. 5049.

[20] E. A. Caridi, T. Y. Chang, K. W. Goossen, and L. F. Eastman, *Appl. Phys. Lett.,* Vol. 56, 1990, p. 659.

[21] K. W. Goossen, E. A. Caridi, T. Y. Chang, J. B. Stark, D. A. B. Miller, and R. A. Morgan, "Observation of Room-Temperature Blue Shift and Bistability in a Strained InGaAs-GaAs <111> Self-electro-optic Effect Device," *Appl. Phys. Lett.,* Vol. 56, 1990, p. 715.

[22] A. S. Pabla, J. L. Sanchez-Rojas, J. Woodhead, R. Grey, J. P. R. David, G. J. Rees, G. Hill, M. A. Pate, P. N. Robson, R. A. Hogg, T. A. Fisher, A. R. K. Willcox, D. M. whittaker, M. S. Skolnick, and D. J. Mowbray, "Tailoring of Internal Fields in InGaAs/GaAs Multiwell Structures Grown on [111]B GaAs," *Appl. Phys. Lett.,* Vol. 63, 1993, p. 752.

[23] Yoshihiro Sugiyama, Yoshiki Sakuma, Shunichi Muto, and Naoki Yokoyama, "Novel InGaAs/GaAs Quantum Dot Structures Formed in Tetrahedral-Shaped Recesses on [111]B GaAs Substrate Using Metalorganic Vapor Phase Epitaxy," *Appl. Phys. Lett.,* Vol. 67, 1995, p. 256.

[24] A. S. Pabla, J. Woodhead, E. A. Khoo, R. Grey, J. P. R. David, and G. J. Rees, "Partial Screening of Internal Electric Fields in Strained Piezoelectric Quantum Well Lasers: Implications for Optoelectronic Integration," *Appl. Phys. Lett.,* Vol. 68, 1996, p. 1595.

[25] Albert Chin and B. C. Lin, "High Optical Quality of Strained [111] B $In_{0.12}Ga_{0.88}As/Al_{0.2}Ga_{0.8}As$ Multiple Quantum Wells," *Appl. Phys. Lett.,* Vol. 68, 1996, p. 2717.

[26] Albert Chin and W. J. Chen, "Observation of Compositional Modulation in [111]A InGaAs Quantum Wells and the Effect on Optical Properties," *Appl. Phys. Lett.*, Vol. 69, 1996, p. 443.

[27] Craig Cooper, David I. Westwood, and Peter Blood, "Laser Diodes in Piezoelectric Quantum-Well Structures," *Appl. Phys. Lett.,* Vol. 69, 1996, p. 2415.

[28] J. L. Sanchez-Rojas, A. Sacedon, E. Calleja, E. Munoz, A. Sanz-Hervas, G. D. Benito, and M. Lopez, *Phys. Rev. B,* Vol. 53, 1996, p. 15469.

[29] Xiong Zhang, Soo-Jin Chua, Shijie Xu, Kok-Boon Chong, and Kentaro Onabe, "Optical Property of a Novel [111]-Oriented Quantum Structure," *Appl. Phys. Lett.,* Vol. 71, 1997, p. 1840.

[30] Mitsuo Takahashi, Manabu Hirai, Kazuhisa Fujita, Norifumi Egami, and Kenichi Iga, "Growth and Fabrication of Strained-Layer InGaAs/GaAs Quantum Well Lasers Grown on GaAs(311)A Substrates Using only a Silicon Dopant," *J. Appl. Phys.*, Vol. 82, 1997, p. 4551.

[31] C. H. Chan, M. C. Chen, H. H. Lin, Y. F. Chen, G. J. Jan, and Y. H. Chen, "Characterization of Piezoelectric [111]B InGAAs/GaAs p-i-n Quantum Well Structures Using Photoreflectance Spectroscopy," *Appl. Phys. Lett.,* Vol. 72, 1998, p. 1208.

[32] C. H. Chan, Y. F. Chen, M. C. Chen, H. H. Lin, and G. J. Jan, "Photoreflectance Spectroscopy of Strained-Layer [111]B InGaAs/GaAs Quantum Well Diodes," *J. Appl. Phys.,* Vol. 84, 1998, p. 1595.

[33] F.-Y. Tsai and C. P. Lee, "InGaAs/GaAs Quantum Dots on [111]B GaAs Substrates," *J. Appl. Phys.*, Vol. 84, 1998, p. 2624.

[34] E. Yablonovitch and E. O. Kane, "Reduction of Lasing Threshold Current Density by the Lowering of Valence Band Effective Mass," *Journal of Lightwave Technology*, Vol. LT-4, 1986, p. 504.

[35] T. Hayakawa, K. Takahashi, M. Kondo, T. Suyama, S. Yamamoto, and T. Hijikata, "Enhancement in Optical Transition in [111]-Oriented GaAs-AlGaAs Quantum Well Structures," *Phys. Rev. Lett.,* Vol. 60, 1988, p. 349.

[36] T. Hayakawa, T. Suyama, K. Takahashi, M. Kondo, S. Yamamoto, and T. Hijikata, "Near-Ideal Threshold Behavior in [111] Oriented GaAs/AlGaAs Quantum Well Lasers," *Appl. Phys. Lett.,* Vol. 52, 1988, p. 339.

[37] Landolt-Börnstein, *Numerical Data and Functional Relationships in Science and Technology, Group III*, Vol. 17, O. Madelung, Ed. Berlin: Springer-Verlag, 1982.

[38] B. W. Kim, *Phys. Rev. B*, Vol. 58, 1998, p. 15766.

[39] Evan O. Kane, "Band Structure of Indium Antimonide," *J. Phys. Chem. Solids*, Vol. 1, 1957, p. 249.

[40] Thomas B. Bahder, "Eight-Band k.p Model of Strained Zinc-Blende Crystals," *Phys. Rev. B,* Vol. 41, 1990, p. 11992.

[41] J. C. Ryan and T. L. Reinecke, "Band Gap Renormalization in Semiconductor Quantum Wells," *Superlattices and Microstructures*, Vol. 13, 1993, p. 177.

[42] T. L. Reinecke, D. A. Broido, E. Lach, V. Kulakovskii, A. Forchel, and D. Gruetzmacher, "Band Gap Renormalization at Finite Carrier Densities in Semiconductor Quantum Wells and Mesa Structures," *Superlattices and Microstructures,* Vol. 7, 1990, p. 437.

[43] L. Hedin and B. I. Lundqvist, *J. Phys. C: Solid State,* Vol. 4, 1971, p. 2064.

[44] P. Vashishta and P. K. Kalia, *Phys. Rev. B*, Vol. 25, 1982, p. 6492.

[45] T. M. Rice, in *Solid State Physics,* Vol. 32, F. Seitz, D. Turnbull, H. Ehrenreich, Ed., Academic, NY, 1977.

[46] B. W. Kim and A. Mjerfeld, "Electronic and Intersubband Optical Properties of p-type GaAs/AlGaAs Superlattices for Infrared Photodetectors," *J. Appl. Phys.,* Vol. 77, 1995, p. 4552.

[47] S. K. Datta, *Quantum Phenomena*, Addison-Wesley, Reading, MA, 1989.

[48] *Numerical Data and Functional Relationships in Science and Technology*, *Group III: Crystal and Solid State Physics, Vol. 22 Semiconductors*, Edited by O. Madelung, Springer-Verlag, New York, 1987.

Byoung-Whi Kim received the Ph.D. degree in electrical and computer engineering from University of Colorado, Boulder, Colorado in 1993. From 1983 to 1988, he was involved in the development of a digital switching system in ETRI. Since he joined ETRI again in 1994, he has been working on III-V compound-semiconductor optical switches based on strain-induced piezoelectric effects. His research interests include theoretical physics of compound semiconductor materials and optoelectronic devices.

Jea-Hoon Yoo received the B.S. and M.S. degrees in electronics engineering from Konkuk University, Seoul, Korea, in 1980 and 1982, respectively. He joined ETRI in 1980, and he worked on the design of telecommunication network until 1983. During the years from 1984 to 1998, he worked in Telecommunications System Department. He has currently served as Manager of Intellectual Property Management Team of ETRI. His research interest centers on technologies of mobile communications.

Soo Hyung Kim received the B.S. and M.S. degrees in electronics engineering from Yonsei University, Seoul, Korea in 1977 and in 1981, respectively, and the Ph. D. degree in information communication engineering from Chungbuk University in 1999. From 1977 to 1983 he was with ETRI, where he was involved in the research of digital exchange systems. In 1984 he moved to Korea Telecom and since then he has played important roles in various national projects in relation to establishing broadband and high-speed telecommunications and data communication networks of Korea. Currently he has served as Managing Director of the Data Network Construction Team of Korea Telecom. His major research interest lies in the technologies to provide Internet services through high-speed ATM networks.